Acta Crystallographica Section B
Structural Science, Crystal Engineering and Materials
ISSN 2052-5206

Comparison of the structural motifs and packing arrangements of six novel derivatives and one polymorph of 2-(1-phenyl-1*H*-1,2,3-triazol-4-yl)pyridine

Kinaan M. Tawfiq,[a,b] Gary J. Miller,[c] Mohamad J. Al-Jeboori,[d] Paul S. Fennell,[d] Simon J. Coles,[e] Graham J. Tizzard,[e] Claire Wilson[f] and Herman Potgieter[g]*

[a]Division of Chemistry and Environmental Sciences, School of Science and the Environment, Manchester Metropolitan University, Chester Street, Manchester M1 5GD, England, [b]Department of Chemistry, College of Education for Pure Sciences – Ibn Al-Haitham, University of Baghdad, Iraq, [c]Analytical Sciences, Manchester Metropolitan University, Chester Street, Manchester M1 5GD, England, [d]Department of Chemical Engineering and Chemical Technology, Imperial College London, London SW7 2AZ, England, [e]EPSRC National Crystallography Service, School of Chemistry, University of Southampton, Southampton SO17 1BJ, England, [f]Diamond Light Source Ltd, Diamond House, Harwell Science and Innovation Campus, Didcot, Oxfordshire OX11 0DE, England, and [g]School of Research, Enterprise and Innovation, Manchester Metropolitan University, Chester Street, Manchester M1 5GD, England

Correspondence e-mail: h.potgeiter@mmu.ac.uk

Received 3 June 2013
Accepted 16 January 2014

The crystal structures of a new polymorph and seven new derivatives of 2-(1-phenyl-1*H*-1,2,3-triazol-4-yl)pyridine have been characterized and examined along with three structures from the literature to identify trends in their intermolecular contact patterns and packing arrangements in order to develop an insight into the crystallization behaviour of this class of compound. Seven unique C—H$\cdots$*X* contacts were identified in the structures and three of these are present in four or more structures, indicating that these are reliable supramolecular synthons. Analysis of the packing arrangements of the molecules using *XPac* identified two closely related supramolecular constructs that are present in eight of the 11 structures; in all cases, the structures feature at least one of the three most common intermolecular contacts, suggesting a clear relationship between the intermolecular contacts and the packing arrangements of the structures. Both the intermolecular contacts and packing arrangements appear to be remarkably consistent between structures featuring different functional groups, with the expected exception of the carboxylic acid derivative 4-(4-(pyridin-2-yl)-1*H*-1,2,3-triazol-1-yl) benzoic acid (L11), where the introduction of a strong hydrogen-bonding group results in a markedly different supramolecular structure being adopted. The occurrence of these structural features has been compared with the packing efficiency of the structures and their melting points in order to assess the relative favourability of the supramolecular structural features in stabilizing the crystal structures.

1. Introduction

The rational design of crystalline systems with specific structures and physical properties is of critical importance for the development of new functional materials such as pharmaceuticals, catalysts, non-linear optics and hydrogen storage materials amongst others (Datta & Grant, 2004; Almarsson & Zaworotko, 2004; Aakeroy *et al.*, 1993; Wong *et al.*, 1997). The *ab initio* design of such materials depends on developing an understanding of the relationship between the directional and non-directional interactions that arise as a consequence of the molecular structure of the components and how these in turn determine and stabilize the supramolecular structure of the resultant crystalline lattice. Traditionally the focus has been on directional intermolecular contacts such as hydrogen and ionic bonds as these are the most readily observable from a visual inspection of a crystal structure (Saha *et al.*, 2005; Desiraju, 1997).

While these interactions are undoubtedly of great importance given their strength and directionality, other non-directional interactions and packing effects also play a major role but can be difficult to identify visually. The *XPac*

(Gelbrich & Hursthouse, 2005) method enables the identification of similarities in the packing arrangements of molecules in related crystal structures that are indicative of common intermolecular interactions and packing effects without limiting the examination to a particular type of interaction. The 'holistic' view of the supramolecular structure afforded by this method promotes a more comprehensive understanding of the relationship between molecular and supramolecular structure in polymorphs, solvates and series of related molecules (Arlin *et al.*, 2010; Gelbrich *et al.*, 2008; Hursthouse *et al.*, 2010, 2011). A complementary approach is the examination of intermolecular contacts by Hirshfeld surface analysis as implemented in *CrystalExplorer* (McKinnon *et al.*, 2007) and when employed in tandem the two methods enable detailed investigation into the supramolecular structure of crystalline systems.

Here we present the crystal structures of a series of related novel 2-pyridyl-1,2,3-triazole derivatives that have been synthesized for use as ligands in the formation of transition metal complexes that can be used in the fabrication of a solar cell. A diverse range of these ligands can be accessed using the Click methodology with an appropriately substituted azide to insert a variety of functional groups into the structure with the concomitant modification of the ligand's steric and electronic properties. The ligands are capable of chelating transition metal atoms and the N atoms are also capable of acting as hydrogen acceptors or as sites for protonation or methylation, while the methine hydrogen of the triazole group is also a good hydrogen-bond donor as a result of the strongly dipolar nature of the heterocycle. A range of ligands have been synthesized for the generation of complexes for catalysis, cancer therapy (Bratsos *et al.*, 2011) and luminescence in the solid state and solution (Crowley *et al.*, 2010).

Previous studies by Schweinfurth have led to the crystallization and characterization of 2-(1-phenyl-1*H*-1,2,3-triazol-4-yl)pyridine (L2) (Schweinfurth *et al.*, 2009) along with the related 4-butoxyphenyl (L9) (Schweinfurth *et al.*, 2008) and 4-(*N*,*N*′-dimethylamine) (L10) (Schweinfurth *et al.*, 2011). Our work has furnished us with a novel polymorph of (L2) in addition to six new substituted derivatives that have been crystallized in their free state. This has provided an opportunity for an examination of the relationship between the molecular structures of this class of compounds and the supramolecular structures adopted in the crystalline state.

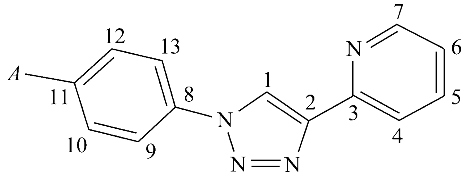

2. Experimental

All reagents were commercially available and used without further purification. Solvents were distilled from appropriate drying agents immediately prior to use. The aryl azide precursors were prepared by published methods (Kamalraj *et al.*, 2008; Nicolaides *et al.*, 2001; Odlo *et al.*, 2008).

IR spectra were recorded as attenuated total reflectance (ATR) using a smart diamond ATR attachment on a Thermo-Nicolet FT–IR spectrometer (AVATAR 320) in the range 4000–500 cm^{-1}. Electronic spectra were measured between 245 and 400 nm with $10^{-3}M$ solutions in dimethylsulfoxide (DMSO) spectroscopic grade solvent at 294 K using a Perkin–Elmer spectrophotometer Lambda. Mass spectra were obtained by HRMS (P + NSI) and HRMS (P − NSI) and in the case of (L3) using a Thermo LTQ Orbitrap XL spectrometer. NMR spectra (^{1}H, ^{13}C, DEPT, ^{1}H–^{1}H COSY, ^{13}C–^{1}H HMQC NMR) were acquired in CD_2Cl_2 or in DMSO-d_6 for (L11) solutions using a JEOL Lambda 400 MHz spectrometer with tetramethylsilane (TMS) for ^{1}H NMR spectra.

2.1. Synthesis

All the compounds were synthesized by a standard literature procedure with small modifications as necessary (Crowley *et al.*, 2010, 2011; Kumar & Reddy, 2010; Park *et al.*, 2008). The ^{1}H and ^{13}C NMR assignments are based on the general numbering pattern used for the assignments of the NMR data, where A = H in (L1) and (L2), F in (L3), Cl in (L4), CH_3 in (L5), CF_3 in (L6), CN in (L7), OCH_3 in (L8), $O(CH_2)_3CH_3$ in (L9), $N(CH_3)_2$ in (L10) and CO_2H in (L11).

2.1.1. Preparation of 2-(1-phenyl-1*H*-1,2,3-triazol-4-yl)pyridine (L1) (Crowley *et al.*, 2010, 2011; Schweinfurth *et al.*, 2009). A mixture of 1-azidobenzene (0.75 g, 6.29 mmol) and 2-ethynylpyridine (0.77 g, 7.75 mmol, 1.2 equiv.) was dissolved in a 1:1 mixture of water/*tert*-butyl alcohol (100 ml). After stirring for 20 min, a solution of $CuSO_4 \cdot 5H_2O$ (0.41 g, 1.64 mmol) in water (10 ml) was added dropwise, followed by a freshly prepared solution of sodium ascorbate (0.37 g, 1.85 mmol) in water (5 ml). The mixture was allowed to stir for 24 h at room temperature, and then an aqueous ammonia solution (15%, 50 ml) was added. The mixture was stirred for a further 20 min, and then extracted with CH_2Cl_2 (2 × 100 ml). The organic phase was washed twice with water (2 × 100 ml) and filtered through celite to remove trapped Cu^I salts $[Cu(NH_3)_6]^+$. The combined organic layer was washed with brine (2 × 100 ml), dried over $MgSO_4$, filtered and evaporated *in vacuo* to give the crude product as a pale yellow solid (1.17 g, 84%). Recrystallization from a mixture of CH_2Cl_2:CH_3OH (1/1) gave a colourless solid in 80% yield (1.12 g, 5.04 mmol), m.p. 361–363 K. IR: ν (cm^{-1}): 3116, 3051, 3001, 1599, 1591, 1567, 1544, 1502, 1471, 1405, 1354, 1237, 1189, 1147, 1091, 1035, 913, 843, 792 and 756. UV–vis (DMSO) λ_{max}: 284 nm, ϵ_{max} = 24375 $dm^3\ mol^{-1}\ cm^{-1}$. ^{1}H NMR (400 MHz, CD_2Cl_2) δ_H (p.p.m.): 8.62 (1H, s, C—H1—triazole), 8.61–8.59 (1H, ddd, $^1J_{HH}$ = 0.92 Hz, $^2J_{HH}$ = 1.83 Hz, $^3J_{HH}$ = 5.04 Hz, C7—H7—*py*), 8.21–8.19 (1H, td, ^1J = 0.92 Hz, ^2J = 2.29 Hz, $^3J_{HH}$ = 8.24, C4—H4—py), 7.84–7.79 (3H, m, C5—H5—*py*, Ar—*Ph*, C—H9, C—H13), 7.59–7.55 (2H, d, J = 7.73 Hz, *Ar*—*Ph*, C—H10, C—H12), 7.50–7.45 (1H, ttt, ^1J = 0.92 Hz, ^2J = 1.73 Hz, $^3J_{HH}$ = 7.73 Hz, C11—H11—*py*), 7.28–7.24 (1H, ddd, $^1J_{HH}$ = 1.73 Hz, $^2J_{HH}$ = 5.04 Hz, ^3J = 7.33 Hz, C6—H6—*py*). ^{13}C NMR

(400 MHz, in CD_2Cl_2) δc (p.p.m.): 120.39 (C_1—triazole), 120.41 (C4—*py*), 120.72 (C9, C13—*Ar*—*Ph*), 123.35 (C6—*py*), 129.12 (C11—*Ar*—*Ph*), 130.11 (C10, C12—*Ar*—*Ph*), 137.18 (C5—*py*), 137.39 (C8—*Ar*—*Ph*), 149.29 (C2—triazole), 149.92 (C7—*py*), 150.39 (C3—*py*). Accurate electrospray mass spectroscopy (ESI): *m*/*z* 223.0977 $[M+H]^+$ (100%) for ($C_{14}H_{12}N_4$), requires = 223.0978, 195.0915 $[(M-N_2) + H]^+$ (35%). Crystals of suitable quality for single-crystal X-ray diffraction were obtained by slow evaporation of a 1:1 CH_2Cl_2:CH_3OH solution of the ligand.

2.1.2. Preparation of 2-(1-(4-fluorophenyl)-1*H*-1,2,3-triazol-4-yl)pyridine (L3). The method used was analogous to that for (L1), but with 1-azido-4-fluorobenzene (0.80 g, 5.83 mmol) in place of phenyl azide. The quantities of the other reagents were adjusted accordingly. An identical work-up procedure gave the required compound as a colourless solid. Yield: 1.17 g (83%), m.p. 451–453 K. IR: ν (cm^{-1}): 3151, 3072, 3025, 1598, 1572, 1549, 1515, 1472, 1405, 1359, 1300, 1220, 1189, 1163, 1150, 1101, 1035, 994, 844 and 782; UV–vis (DMSO) λ_{max}: 282 nm, ϵ_{max} = 19880 $dm^3\ mol^{-1}\ cm^{-1}$. ^{1}H NMR (400 MHz, CD_2Cl_2) δ_H (p.p.m.): 8.60–8.59 (1H, dd, J_{HH} = 4.58 Hz, C_7—H7—*py*), 8.58 (1H, s, H1, C_1—H1—triazole), 8.20–8.18 (1H, d, J_{HH} = 7.79 Hz, C_4—H4—*py*), 7.84–7.78 (3H, m, C_5—H5—*py*, *Ar*—*Ph*, C—H9, C—H13), 7.73–7.70 (td, J_{H-F}, $^1J_{HH}$ = 2.29 Hz, $^2J_{HH}$ = 3.21 Hz, $^3J_{HH}$ = 9.16 Hz), 7.29–7.24 (3H, m, C_6—H6—*py*, *Ar*—*Ph*, C—H10, C—H12), 7.07–7.04 (td, J_{H-F}, $^1J_{HH}$ = 1.83 Hz, $^2J_{HH}$ = 3.66 Hz, $^3J_{HH}$ = 8.70 Hz); ^{13}C NMR (400 MHz, CD_2Cl_2) δC (p.p.m.): 116.98–117.20 ($^2J_{C-F}$ = 23.00 Hz, C_{10}, C12—*Ar*—*Ph*), 120.48 (C1—triazole), 120.69 (C4—*py*), 122.85–122.93 (d, $^3J_{C-F}$ = 8.63 Hz, C9, C13—*Ar*—*Ph*), 123.51 (C6—*py*), 133.82 (C8—*Ar*—*Ph*), 137.29 (C5—*py*), 149.51 (C2—triazole), 150.02 (C7—*py*), 150.37 (C3—*py*), 161.65–164.12 $^1J_{C-F}$ = 248.24 Hz (C11—*Ar*—*Ph*). Accurate electrospray mass spectroscopy: *m*/*z* 241.0885 $[M+H]^+$ (100%) for ($C_{14}H_{12}N_4F$), requires = 241.0884, 213.0823 $[(M-N_2)+H]^+$ (15%). Crystals of suitable quality for single-crystal X-ray diffraction were obtained by slow evaporation of a 1:1 C_3H_6O:CH_3OH solution of the ligand.

2.1.3. Preparation of 2-(1-(4-chlorophenyl)-1*H*-1,2,3-triazol-4-yl)pyridine (L4) (Park *et al.*, 2008; Wolff *et al.*, 2013). The method used was similar to that for (L1), but with 1-azido-4-chlorobenzene (0.65 g, 4.23 mmol) in place of phenyl azide. The quantities of the other reagents were adjusted accordingly. An identical work-up procedure gave the required compound as a colourless solid. Yield: 0.87 g (81%), m.p. 476–478 K. IR: ν (cm^{-1}): 3132, 3058, 1602, 1589, 1570, 1570, 1550, 1473, 1440, 1421, 1399, 1355, 1236, 1174, 1145, 1114, 1091, 1037, 996, 817, 779 and 739. UV–vis (DMSO) λ_{max}: 284 nm, ϵ_{max} = 23925 $dm^3\ mol^{-1}\ cm^{-1}$. ^{1}H NMR (400 MHz, CD_2Cl_2) δ_H (p.p.m.): 8.60 (1H, s, C_1—H1—triazole), 8.59–8.58 (1H, ddd, $^1J_{HH}$ = 0.92 Hz, $^2J_{HH}$ = 1.83 Hz, $^3J_{HH}$ = 5.04, C7—H7—*py*), 8.20–8.18 (1H, dd, ^1J = 0.92 Hz, $^2J_{HH}$ = 7.79 Hz, C4—H4—*py*), 7.83–7.76 (3H, m, C5—H5—*py*, *Ar*—*Ph*, C—H13, C—H9), 7.56–7.52 (2H, d, J_{HH} = 9.16 Hz, *Ar*—Ph, C—H12, C—H10), 7.28–7.25 (1H, ddd, $^1J_{HH}$ = 0.92 Hz, $^2J_{HH}$ = 5.04 Hz, $^3J_{HH}$ = 7.79 Hz, C_6—H6—*py*); ^{13}C NMR (400 MHz, CD_2Cl_2) δC (p.p.m.): 120.42 (C1—triazole), 120.57 (C4—*py*), 122.04 (C9, C13—Ar—*Ph*), 123.54 (C6—*py*), 130.33 (C10, C12—*Ar*—*Ph*), 134.80 (C8—*Ar*—*Ph*), 136.01 (C11—*Ar*—*Ph*), 137.30 (C5—*py*), 149.57 (C2—triazole), 150.00 (C7—*py*), 150.26 (C3—*py*). Accurate electrospray mass spectroscopy: *m*/*z* 257.0590 $[M+H]^+$ (100%) for ($C_{13}H_{19}N_3Cl$), requires = 257.0589; 229.0528 $[(M+H)-(N_2)]^+$ (25%). Crystals of suitable quality for single-crystal X-ray diffraction were obtained by slow evaporation of a 1:1 C_3H_6O:CH_3OH solution of the ligand.

2.1.4. Preparation of 2-(1-(*p*-tolyl)-1*H*-1,2,3-triazol-4-yl)pyridine (L5) (Kumar & Reddy, 2010). This ligand was prepared in the same manner as that for (L1) using 1-azido-4-methylbenzene (0.75 g, 5.63 mmol) in place of phenyl azide. The quantities of the other reagents were adjusted accordingly. An identical work-up procedure gave the required compound as a colourless solid. Yield: 0.93 g (70%), m.p. 401–402 K. IR: ν (cm^{-1}): 3128, 3099, 2947, 2919, 1597, 1592, 1566, 1549, 1471, 1271, 1238, 1212, 1176, 1148, 1031, 998, 813, 784 and 745. UV–vis (DMSO) λ_{max}: 283 nm, ϵ_{max} = 17200 $dm^3\ mol^{-1}\ cm^{-1}$. ^{1}H NMR (400 MHz, $CDCl_3$) δH (p.p.m.): 8.60–8.58 (1H, ddd, $^1J_{HH}$ = 0.92 Hz, $^2J_{HH}$ = 1.83 Hz, $^3J_{HH}$ = 5.04 Hz, C7—H7—*py*), 8.57 (1H, s, C_1—H1—triazole), 8.21–8.18 (1H, td, $^1J_{HH}$ = 0.92 Hz, $^2J_{HH}$ = 7.79 Hz, C4—H4—*py*), 7.82–7.77 (1H, td, $^1J_{HH}$ = 1.83 Hz, $^2J_{HH}$ = 7.79 Hz, C5—H5—*py*), 7.70–7.67 (2H, d, J_{HH} = 8.70 Hz, *Ar*—*Ph*, C—H9, C—H13), 7.35–7.33 (2H, d, J_{HH} = 8.24 Hz, *Ar*—*Ph*, C—H10, C—H12), 7.26–7.23 (1H, dd, $^1J_{HH}$ = 0.92 Hz, $^2J_{HH}$ = 5.04 Hz, ^3J = 7.33, C6—H6—*py*), 2.41 (3H, s, C—H, CH_3); ^{13}C NMR (400 MHz, $CDCl_3$) δC (p.p.m.): 21.14 (C—CH_3), 120.34 (C5—*py*), 120.37 (C1—triazole), 120.56 (C9, C13—*Ar*—*Ph*), 123.26 (C6—*py*), 130.56 (C10, C12—*Ar*—*Ph*), 135.05 (C11—*Ar*—*Ph*), 137.13 (C5—*py*), 139.40 (C1—*py*), 149.14 (C2—triazole), 149.89 (C7—*py*), 150.48 (C3—*py*). Accurate electrospray mass spectroscopy: *m*/*z* 237.1133 $[M+H]^+$ (100%) for ($C_{14}H_{12}N_4$), requires = 237.1135, 209.1133 $[(M-N_2)+H]^+$ (15%). Crystals of suitable quality for single-crystal X-ray diffraction were obtained by slow evaporation of a 1:1 C_3H_6O:CH_3OH solution of the ligand.

2.1.5. Preparation of 2-(1-(4-(trifluoromethyl)phenyl)-1*H*-1,2,3-triazol-4-yl)pyridine (L6) (Schweinfurt *et al.*, 2011). The method used was similar to that for (L1), but with 1-azido-4-trifluoromethylbenzene (0.5 g, 2.67 mmol) in place of phenyl azide. The quantities of the other reagents were adjusted accordingly. An identical work-up procedure gave the required compound as a colourless solid. Yield: 0.58 g (75%), m.p. 441–443 K. IR: ν (cm^{-1}): 3122, 3060, 1615, 1593, 1570, 1547, 1528, 1472, 1409, 1322, 1279, 1237, 1191, 1161, 1104, 1066, 1027, 991, 847, 785, 746 and 694. UV–vis (DMSO) λ_{max}: 288 nm, ϵ_{max} = 14980 $dm^3\ mol^{-1}\ cm^{-1}$. ^{1}H NMR ($CDCl_3$) δH (p.p.m.): 8.70 (1H, s, C_1—H1—triazole), 8.61–8.60 (1H, td, $^1J_{HH}$ = 0.95 Hz, ^2J = 1.83 Hz, ^3J = 4.58 Hz, C7—H7—*py*), 8.21–8.19 (1H, d, J_{HH} = 7.79 Hz, C4—H4—*py*), 8.01–7.99 (2H, d, J_{HH} = 8,70 Hz, *Ar*—*Ph*, C—H9, C—H13), 7.85–7.78 (3H, m, *Ar*—*Ph*, C—H10, C—H12, C5—H5—*py*), 730–7.26 (1H, m, $^1J_{HH}$, C6—H6—*py*). ^{13}C NMR (400 MHz, $CDCl_3$) δC (p.p.m.): 119.69 (C1—triazole), 120.29 (C9, C13—*Ar*—*Ph*), 119.43, 122.14, 124.85, 127.27 (q, J_{C-F} = 270.20 Hz, CF_3), 120.51 (C4—

py), 123.85 (C6—*py*), 127.11, 127.14, 127.18, 127.21 (q, $^{3}J_{C-F}$ = 3.83 Hz, C10, C14—*Ar*—*Ph*), 130.28, 130.61, 130.94, 131.27 (q, $^{2}J_{C-F}$ = 32.59 Hz, C—CF$_3$ (C11—*Ar*—*Ph*), 137.04 (C5—*py*), 139.31 (C8—*Ar*—*Ph*), 149.39 (C2—triazole), 149.51 (C3—*py*), 149.55 (C7-py). Accurate electrospray mass spectroscopy: *m*/*z* 291.0853 [*M*+H]$^+$ (100%) for ($C_{14}H_9N_4F_3$), requires = 291.0852, 263.0794 [(*M*—N$_2$) + H]$^+$ (20%). Crystals of suitable quality for single-crystal X-ray diffraction were obtained by slow evaporation of a 1:1 C_3H_6O:CH_3OH solution of the ligand.

2.1.6. Preparation of 4-(4-(pyridin-2-yl)-1*H*-1,2,3-triazol-4-yl)benzonitrile (L7) (Alonso *et al.*, 2011; Park *et al.*, 2008; Park & Park, 2011). The method used was analogous to that for (L1), but with 1-azido-4-methoxy benzene (1 g, 6.70 mmol) in place of phenyl azide. The quantities of the other reagents were adjusted accordingly. An identical work-up procedure gave the required compound as a colourless solid. Yield: 1.57 g (93%), m.p. 402–403 K. IR: ν (cm^{-1}): 3142, 3006, 2844, 1604, 1592, 1574, 1549, 1551, 1515, 1275, 1258, 1237, 1174, 1089, 1023, 996, 823 and 777. UV–vis (DMSO) λ_{max}: 285 nm, ϵ_{max} = 24375 dm^3 mol^{-1} cm^{-1}. ^{1}H NMR (400 MHz, DCM) δH (p.p.m.): 8.60–8.58 (1H, d, $^{1}J_{HH}$ = 0.92 Hz, $^{2}J_{HH}$ = 1.83 Hz, $^{3}J_{HH}$ = 5.50 Hz, C7—H7—*py*), 8.53 (1H, s, C1—H1—triazole), 8.20–8.18 (1H, d, $^{1}J_{HH}$ = 0.92 Hz, $^{2}J_{HH}$ = 7.79 Hz, C4—H4—*py*), 7.83–7.79 (1H, dt, $^{1}J_{HH}$ = 1.83 Hz, ^{2}J = 7.79 Hz, C5—H5—*py*), 7.74–7.70 (2H, d, *J* = 9.16 Hz, *Ar*—*Ph*, C—H9, C—H13), 7.28–7.24 (1H, ddd, $^{1}J_{HH}$ = 1.73 Hz, $^{2}J_{HH}$ = 4.58 Hz, $^{3}J_{HH}$ = 7.33, C6—H6—*py*), 7.08–7.06 (2H, d, J_{HH} = 9.16 Hz, *Ar*—*Ph*, C—H10, C—H12), 3.88 (3H, s, CH$_3$); ^{13}C NMR (400 MHz, DMSO-d$_6$) δC (p.p.m.): 56.06 (C—CH$_3$), 115.17 (C10, C12—*Ar*—*Ph*), 120.42 (C4—*py*), 120.64 (C1—triazole), 122.45 (C9, C$_{13}$—*Ar*—*Ph*), 123.35 (C6—*py*), 130.89 (C8), 137.25 (C5—*py*), 149.18 (C2—triazole), 149.97 (C7—*py*), 150.62 (C3—*py*), 160.38 (C14—*Ar*—*Ph*). Accurate electrospray mass spectroscopy: *m*/*z* 253.1082 [*M*+H]$^+$ (100%) for ($C_{14}H_{12}N_4O$), requires = 253.1084. Crystals of suitable quality for single-crystal X-ray diffraction were obtained by slow evaporation of a 1:1 CH_2Cl_2:CH_3OH solution of the ligand.

2.1.7. Preparation of 2-(1-(4-methoxy-phenyl)-1*H*-1,2,3-triazol-1-yl)pyridine (L8). The method used was similar to that for (L1), but with 1-azido-4-methoxy benzene (1 g, 6.70 mmol) in place of phenyl azide. The quantities of the other reagents were adjusted accordingly. An identical work-up procedure gave the required compound as a colourless solid. Yield: 1.51 g (91%), m.p. 517–519 K. IR: ν (cm^{-1}): 3120, 3079, 2229, 1601, 1572, 1572, 1549, 1511, 1470, 1446, 1351, 1274, 1235, 1178, 1147, 1032, 998, 849, 782 and 742. UV–vis (DMSO) λ_{max}: 292 nm, ϵ_{max} = 24375 dm^3 mol^{-1} cm^{-1}. ^{1}H NMR (400 MHz, CD_2Cl_2) δH (p.p.m.): 8.70 (1H, s, C1—H1—triazole), 8.62–8.60 (1H, ddd, $^{1}J_{HH}$ = 0.92 Hz, $^{2}J_{HH}$ = 1.83 Hz, $^{3}J_{HH}$ = 5.95, C7—H7—*py*), 8.22–8.20 (1H, td, ^{1}J = 0.92 Hz, $^{2}J_{HH}$ = 1.37 Hz, ^{3}J = 7.79 Hz, C4—H4—*py*), 8.01–7.99 (2H, d, *J* = 8.70, *Ar*—*Ph*, C—H9, C—H13), 7.89–7.87 (2H, d, J_{HH} = 8.70 Hz, *Ar*—*Ph*, C—H10, C—H12), 7.86–7.82 (1H, dt, ^{1}J = 1.83 Hz, ^{2}J = 7.79 Hz, C5—H5—*py*), 7.30–7.26 (1H, ddd, $^{1}J_{HH}$ = 0.92 Hz, $^{2}J_{HH}$ = 4.58 Hz, $^{3}J_{HH}$ = 7.79 Hz, C6—H6—*py*); ^{13}C NMR (400 MHz, CD_2Cl_2) δC (p.p.m.): 112.77 (C—CN), 118.21 (C11—*Ar*—*Ph*), 120.23 (C1—triazole), 120.65 (C4—*py*), 120.93 (C9, C13—*Ar*—*Ph*), 123.73 (C6—*py*), 134.84 (C10, C12—*Ar*—*Ph*), 137.39 (C5—*py*), 140.21 (C8—*Ar*—*Ph*), 149.93 (C2—triazole), 150.02 (C3—*py*), 150.02 (C7—*py*). Accurate electrospray mass spectroscopy: *m*/*z* 248.0933 [*M*+H]$^+$ (100%) for ($C_{14}H_{12}N_4$), requires = 248.0932, 220.0871 [(*M*—N$_2$)+H]$^+$ (55%). Crystals of suitable quality for single-crystal X-ray diffraction were obtained by slow evaporation of a 1:1 CH_2Cl_2:CH_3OH solution of the ligand.

2.1.8. Preparation of 4-(4-(pyridin-2-yl)-1*H*-1,2,3-triazol-1-yl) benzoic acid (L11). The method used was analogous to that for (L1), but with 4-azido benzoic acid (1 g, 6.13 mmol) in place of phenyl azide. The quantities of the other reagents were adjusted accordingly. An identical work-up procedure gave the required compound as a colourless solid. Yield: 1.24 g (76%); m.p. 610–612 K. IR: ν (cm^{-1}); 3141, 3003, 1687, 1603, 1588, 1573, 1549, 1553, 1403, 1302, 1269, 1240, 1258, 1174, 1089, 1023, 991, 856, 768 and 692. UV–vis (DMSO) λ_{max}: 291 nm, ϵ_{max} = 81400 dm^3 mol^{-1} cm^{-1}. ^{1}H NMR (400 MHz, DMSO-d$_6$) δH (p.p.m.): 13.27 (1H, s, —COOH), 9.46 (1H, s, C1—H—triazole), 8.69–8.67 (1H, d, *J* = 4.02 Hz, C7—H—*py*), 8.22–8.13 (5H, m, C4—H—*py*, Ar—*Ph*, H 9, 13, 10, 12), 7.99–7.94 (1H, dt, ^{1}J = 1.93 Hz, ^{2}J = 7.63 Hz, C5—H—*py*), 7.44–7.41 (1H, dd, $^{1}J_{HH}$ = 6.48 Hz, $^{2}J_{HH}$ = 7.25 Hz, C6—H—*py*); ^{13}C NMR (400 MHz, DMSO-d$_6$) δC (p.p.m.): 119.94 (C4—*py*, C10, C12—*Ar*—*Ph*), 121.41 (C1—triazole), 123.48 (C6—*py*), 131.03 (C9, C13—Ar—*Ph*), 130.17 (C11—*Ar*—*Ph*), 137.37 (C—*py*), 139.46 (C8—*Ar*—*Ph*), 148.43 (C3—triazole), 149.26 (C2—*py*), 149.72 (C7—*py*), 166.39 (C—COOH). Accurate electrospray mass spectroscopy: *m*/*z* 264.0774 [*M*—H]$^-$ (100%) for $C_{14}H_{10}N_4O_2$, requires = 264.0778, 191.0198 [(*M*—N$_2$)—H]$^-$ (10%). Crystals of suitable quality for single-crystal X-ray diffraction were obtained by slow evaporation of a 1:4:4 DMSO:CH_3OH:CH_3CN solution of the ligand.

2.2. Data collection, structure solution and refinement

For each sample suitable single crystals were mounted on glass fibres and held at 120 K under a nitrogen flow from an Oxford Cryosystems Cryostream 700. Single-crystal X-ray diffraction data for (L1), (L4), (L5) and (L6) were collected using a Nonius–Kappa CCD area detector mounted at the window of an FR591 rotating anode generator (Mo $K\alpha$, λ = 0.71073 Å). Data were processed using *COLLECT* (Nonius, 1998) and the unit-cell parameters were refined against all data. An empirical absorption correction was carried out using *SADABS* (Bruker, 2007) and the structures were solved by the charge-flipping algorithm using *SUPERFLIP* (Palatinus & Chapuis, 2007). Data for (L7), (L8) and (L11) were collected using a Rigaku Saturn 724+ area detector mounted at the window of an FR-E+ rotating anode generator (Mo $K\alpha$, λ = 0.71073 Å) and (L3) was collected using a Rigaku R-axis Spider image-plate detector with a sealed-tube source (Mo $K\alpha$, λ = 0.71073 Å). These data were processed and empirical absorption corrections were carried out using *CrystalClear SM-Expert* (Rigaku, 2011). The structures were solved by direct methods using *SHELXS97* (Sheldrick, 2008)

Table 1
Crystallographic data for the novel structures characterized in this work.

Experiments were carried out with Mo $K\alpha$ radiation. H-atom parameters were constrained.

	(L1)	(L3)	(L4)	(L5)
Crystal data				
Chemical formula	$C_{13}H_{10}N_4$	$C_{13}H_9FN_4$	$C_{13}H_9ClN_4$	$C_{14}H_{12}N_4$
M_r	222.25	240.24	256.69	236.28
Crystal system, space group	Monoclinic, $P2_1/c$	Monoclinic, $P2_1/c$	Monoclinic, $C2/c$	Monoclinic, $P2_1$
Temperature (K)	120	120	120	120
a, b, c (Å)	22.6348 (5), 5.8250 (1), 17.8421 (4)	12.2031 (3), 7.9798 (2), 11.6329 (3)	16.0000 (11), 5.9258 (2), 24.3829 (17)	5.7797 (5), 6.7414 (4), 15.0259 (12)
α, β, γ (°)	90, 113.007 (1), 90	90, 104.043 (2), 90	90, 93.109 (8), 90	90, 92.359 (4), 90
V (Å^3)	2165.32 (8)	1098.94 (5)	2308.4 (2)	584.96 (8)
Z	8	4	8	2
Radiation type	Mo $K\alpha$	Mo $K\alpha$	Mo $K\alpha$	Mo $K\alpha$
μ (mm^{-1})	0.09	0.10	0.32	0.08
Crystal size (mm)	0.34 × 0.23 × 0.20	0.60 × 0.58 × 0.40	0.36 × 0.12 × 0.06	0.38 × 0.12 × 0.10
Data collection				
Diffractometer	Bruker–Nonius CCD camera on κ-goniostat	Bruker–Nonius CCD camera on κ-goniostat	Rigaku R-AXIS SPIDER IP	Bruker–Nonius CCD camera on κ-goniostat
Absorption correction	Multi-scan *SADABS* 2007/2 (Bruker, 2007)	Multi-scan *SADABS* 2007/2 (Bruker, 2007)	Multi-scan *CrystalClear-SM Expert* 2.0 r13 (Rigaku, 2011)	Multi-scan *SADABS* 2007/2 (Bruker, 2007)
T_{min}, T_{max}	0.971, 0.983	0.940, 0.960	0.608, 1.000	0.969, 0.992
No. of measured, independent and observed [$I > 2\sigma(I)$] reflections	35 200, 4956, 4405	13 725, 2510, 2228	11 996, 2636, 1654	9647, 2622, 2042
R_{int}	0.057	0.031	0.050	0.056
$(\sin \theta/\lambda)_{max}$ (Å^{-1})	0.649	0.649	0.649	0.649
Refinement				
$R[F^2 > 2\sigma(F^2)]$, $wR(F^2)$, S	0.046, 0.108, 1.06	0.038, 0.092, 1.05	0.045, 0.137, 1.04	0.048, 0.124, 1.04
No. of reflections	4956	2510	2636	2622
No. of parameters	309	163	163	165
No. of restraints	0	0	0	1
$\Delta\rho_{max}$, $\Delta\rho_{min}$ (e Å^{-3})	0.27, −0.35	0.26, −0.23	0.25, −0.46	0.17, −0.18

	(L6)	(L7)	(L8)	(L11)
Crystal data				
Chemical formula	$C_{14}H_9F_3N_4$	$C_{14}H_9N_5$	$C_{14}H_{12}N_4O$	$C_{14}H_{10}N_4O_2$
M_r	290.25	247.26	252.28	266.26
Crystal system, space group	Triclinic, $P\overline{1}$	Monoclinic, $C2/c$	Triclinic, $P1$	Monoclinic, $P2_1/c$
Temperature (K)	120	100	100	100
a, b, c (Å)	5.7460 (1), 7.2076 (2), 15.2997 (4)	16.0427 (19), 5.8677 (6), 24.487 (3)	3.7837 (4), 10.8502 (16), 15.2200 (17)	10.5970 (17), 14.471 (2), 7.7343 (12)
α, β, γ (°)	103.045 (2), 98.768 (2), 92.290 (2)	90, 92.354 (8), 90	109.226 (11), 97.056 (6), 91.514 (9)	90, 90.121 (6), 90
V (Å^3)	608.25 (3)	2303.1 (5)	584.03 (12)	1186.0 (3)
Z	2	8	2	4
Radiation type	Mo $K\alpha$	Mo $K\alpha$	Mo $K\alpha$	Mo $K\alpha$
μ (mm^{-1})	0.13	0.09	0.10	0.11
Crystal size (mm)	0.60 × 0.20 × 0.18	0.22 × 0.14 × 0.04	0.16 × 0.04 × 0.01	0.12 × 0.12 × 0.03
Data collection				
Diffractometer	Bruker–Nonius CCD camera on κ-goniostat	Rigaku AFC12	Rigaku AFC12	Rigaku AFC12
Absorption correction	Multi-scan *SADABS* 2007/2 (Bruker, 2007)	Multi-scan *CrystalClear-SM Expert* 2.0 r7 (Rigaku, 2011)	Multi-scan *CrystalClear-SM Expert* 2.0 r13 (Rigaku, 2011)	Multi-scan *CrystalClear-SM Expert* 2.0 r13 (Rigaku, 2011)
T_{min}, T_{max}	0.925, 0.977	0.677, 1.000	0.624, 1.000	0.516, 1.000
No. of measured, independent and observed [$I > 2\sigma(I)$] reflections	14 232, 2785, 2436	9891, 2638, 2154	6395, 2617, 2049	5844, 2705, 1862
R_{int}	0.035	0.061	0.062	0.058
$(\sin \theta/\lambda)_{max}$ (Å^{-1})	0.649	0.649	0.649	0.649
Refinement				
$R[F^2 > 2\sigma(F^2)]$, $wR(F^2)$, S	0.040, 0.109, 1.03	0.046, 0.121, 1.06	0.053, 0.116, 1.08	0.062, 0.161, 1.05
No. of reflections	2785	2638	2617	2705
No. of parameters	191	172	345	182

Table 1 (continued)

	(L6)	(L7)	(L8)	(L11)
No. of restraints	0	0	3	0
$\Delta\rho_{max}$, $\Delta\rho_{min}$ (e Å^{-3})	0.37, −0.30	0.29, −0.25	0.25, −0.29	0.34, −0.29

Computer programs: *CrystalClear-SM Expert* 2.0 r13 (Rigaku, 2011), *DENZO* (Otwinowski & Minor, 1997), *COLLECT* (Nonius, 1998), *SADABS* (Bruker, 2007), *SUPERFLIP* (Palatinus & Chapuis, 2007), *SHELXS97* and *SHELXL97* (Sheldrick, 2008), *OLEX2* (Dolomanov *et al.*, 2009), *WinGX* (Farrugia, 1997).

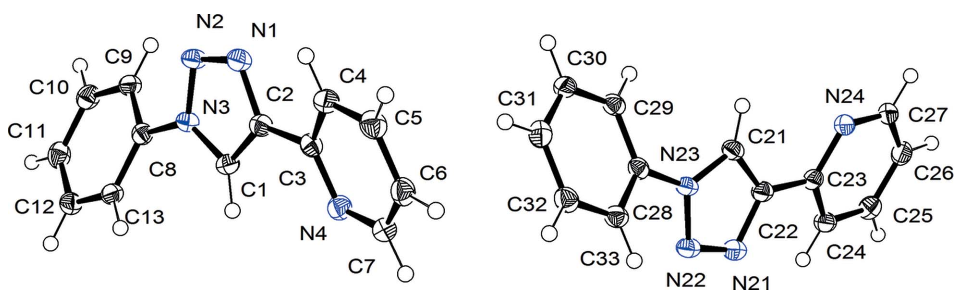

Figure 1
ORTEP view of (L1) with atomic numbering scheme. Displacement ellipsoids are drawn at the 50% probability level. H atoms are presented as small spheres of arbitrary radius.

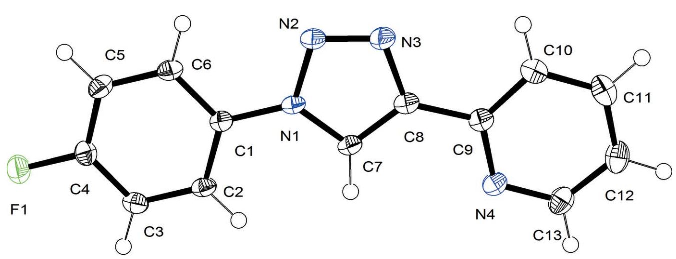

Figure 2
ORTEP view of (L3) with atomic numbering scheme. Displacement ellipsoids are drawn at the 50% probability level. H atoms are presented as small spheres of arbitrary radius.

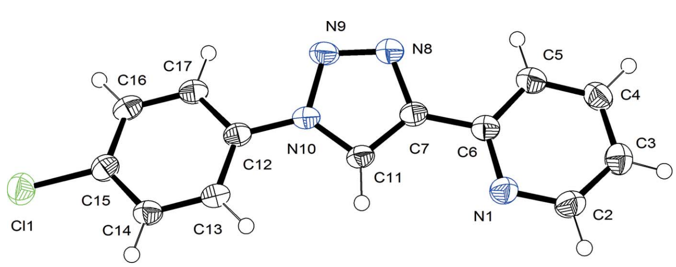

Figure 3
ORTEP view of (L4) with atomic numbering scheme. Displacement ellipsoids are drawn at the 50% probability level. H atoms are presented as small spheres of arbitrary radius.

within *OLEX2* (Dolomanov *et al.*, 2009). All structures were refined on $|F_o|^2$ by full-matrix least squares refinement using *SHELXL97* (Sheldrick, 2008) within *OLEX2*. Detailed crystallographic information is given in Table 1.[1] Non-H atoms were refined anisotropically and H atoms were added at calculated positions and refined using a riding model with C—H (aromatic) 0.95 Å, O—H 0.82 Å with $U_{iso} = 1.2U_{eq}$(C); C—H(methyl) 0.98 Å with $U_{iso} = 1.5U_{eq}$(C).

2.3. Structure analysis

Directional contacts were visualized in *Mercury* (Macrae *et al.*, 2008) using the standard definition for a short contact as atom–atom distances up to the sum of their van der Waals radii. The influence of non-directional interactions and packing effects was assessed by comparing the packing arrangements of the molecules in the structures using *XPac*. Due to the conformational flexibility exhibited by the molecules three comparisons were run using low cut-off parameters, first using all non-H atoms, followed by the non-H atoms of the pyridyl ring and imidazole group, and finally the non-H atoms of the imidazole and phenyl groups. Hirshfeld surfaces were generated using *Crystal-Explorer* (Rigaku, 2011) at the standard high-resolution pixel setting with the X—H distances normalized to standard

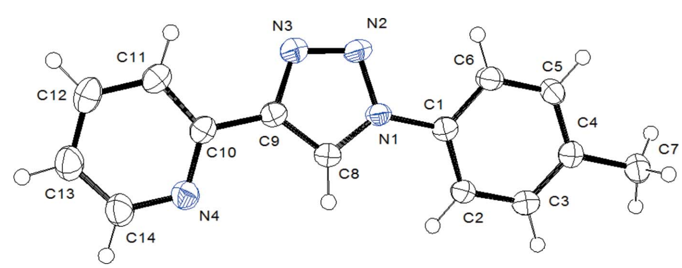

Figure 4
ORTEP view of (L5) with atomic numbering scheme. Displacement ellipsoids are drawn at the 50% probability level. H atoms are presented as small spheres of arbitrary radius.

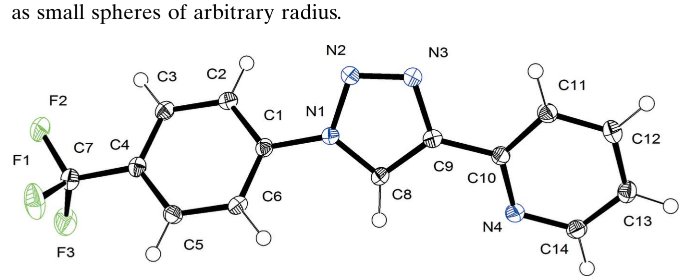

Figure 5
ORTEP view of (L6) with atomic numbering scheme. Displacement ellipsoids are drawn at the 50% probability level. H atoms are presented as small spheres of arbitrary radius.

[1] Supporting information for this paper is available from the IUCr electronic archives (Reference: EB5029).

Table 2
Geometric parameters for the seven C—H···X contacts identified in structures (1)–(10), in cases where more than one crystallographically independent ligand is present in the unit cell details are given for all ligands.

	Contact (I) [(IV) in (L8)]			Contact (II) [(V) in (L8)]			Contact (III) [(VI) in (L8), (VII) in (L9)]		
	C···X (Å)	H···X (Å)	C—H···X (°)	C···X (Å)	H···X (Å)	C—H···X (°)	C···X (Å)	H···X (Å)	C—H···X (°)
(L1*a*)	3.677 (2)	2.739 (1)	169.48 (13)	3.440 (2)	2.679 (1)	137.38 (13)	–	–	–
(L1*b*)	3.660 (2)	2.722 (1)	169.45 (8)	3.377 (2)	2.638 (1)	134.97 (10)	–	–	–
(L2)	3.618 (2)	2.656 (2)	173.7 (1)	3.432 (2)	2.678 (1)	135.9 (1)	–	–	–
(L3)	–	–	–	3.439 (1)	2.536 (1)	159.00 (8)	3.350 (2)	2.449 (1)	158.33 (8)
(L4)	–	–	–	3.202 (3)	2.707 (2)	114.19 (13)	3.450 (3)	2.582 (2)	155.39 (14)
(L5)	–	–	–	3.453 (3)	2.746 (2)	131.87 (14)	–	–	–
(L6)	3.627 (2)	2.713 (1)	161.69 (8)	3.445 (2)	2.664 (1)	139.85 (8)	–	–	–
(L7)	–	–	–	3.151 (2)	2.700 (1)	109.72 (8)	3.476 (2)	2.580 (1)	157.29 (9)
(L8*a*)	3.672 (5)	2.724 (3)	177.4 (3)	3.390 (6)	2.675 (3)	132.4 (2)	3.382 (5)	2.506 (2)	153.4 (3)
(L9*a*)	3.685 (2)	2.737 (1)	175.49 (9)	3.344 (2)	2.626 (1)	132.70 (9)	3.514 (2)	1.714 (1)	142.27 (11)
(L9*b*)	3.662 (2)	2.749 (1)	161.41 (9)	3.282 (2)	2.634 (1)	125.86 (10)	3.631 (2)	2.751 (1)	154.37 (10)
(L10*a*)	3.783 (10)	2.854 (6)	166.0 (5)	–	–	–	–	–	–
(L10*b*)	3.768 (9)	2.818 (5)	177.6 (6)	–	–	–	–	–	–
(L10*c*)	3.859 (10)	3.003 (6)	150.6 (5)	–	–	–	–	–	–
(L10*d*)	3.794 (9)	2.920 (6)	153.5 (5)	–	–	–	–	–	–

neutron diffraction values and Kitaiigorodskii's packing index (KPI) was calculated using *PLATON* (Spek, 2003).

3. Results and discussion

Of the 11 structures examined here, seven crystallized as $Z' = 1$ structures with the new polymorph (L1) and the methoxy and

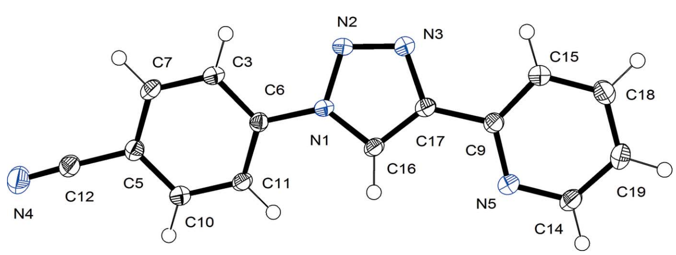

Figure 6
ORTEP view of (L7) with atomic numbering scheme. Displacement ellipsoids are drawn at the 50% probability level. H atoms are presented as small spheres of arbitrary radius.

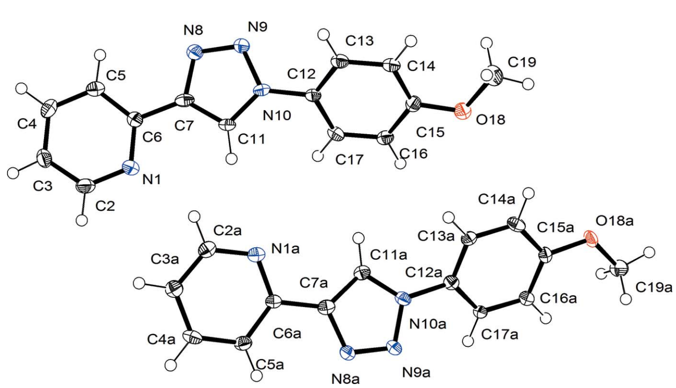

Figure 7
ORTEP view of (L8) with atomic numbering scheme. Displacement ellipsoids are drawn at the 50% probability level. H atoms are presented as small spheres of arbitrary radius.

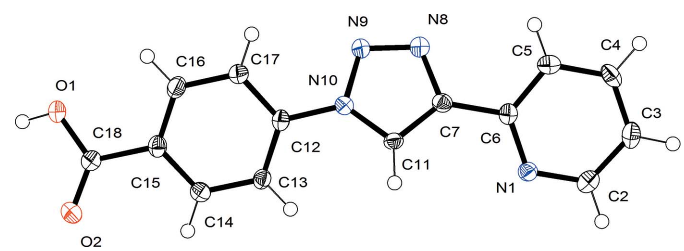

Figure 8
ORTEP view of (L11) with atomic numbering scheme. Displacement ellipsoids are drawn at the 50% probability level. H atoms are presented as small spheres of arbitrary radius.

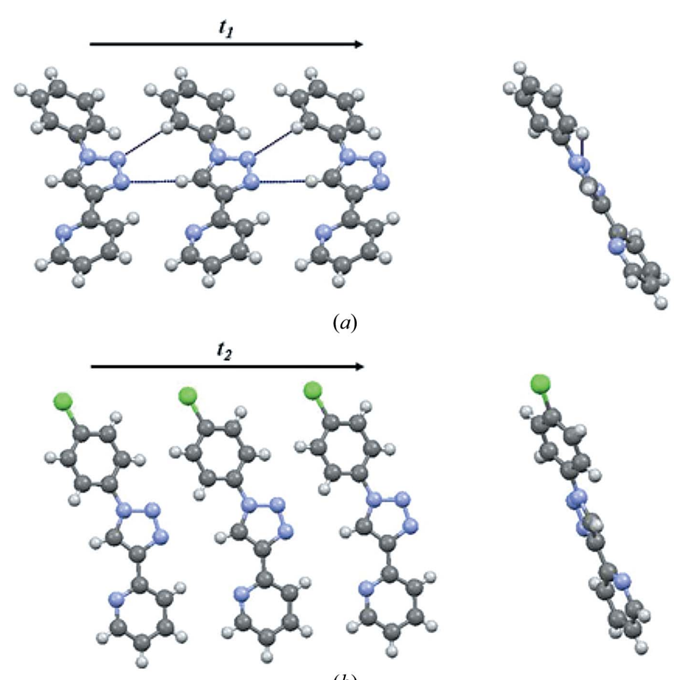

Figure 9
Supramolecular construct *A* as identified in the crystal structure of (L2) (*a*) and *B* in the crystal structure of (L3) (*b*) viewed perpendicular to their translation vectors (left) and along the axes (right). Intermolecular hydrogen bonds in *A* are shown as dark blue lines.

Table 3
Summary of the structural parameters examined for structures (L1)–(L11).

	SC	Hydrogen-bond motifs	Hirshfeld H—H (%)	KPI	M.p. (K)
(L1)	*A*	(I), (II)	36.6/36.0	71.0	362 (1)
(L2)	*A*	(I), (II)	38.7	71.4	Unknown
(L3)	*B*	(II), (III)	32.8	71.1	470 (1)
(L4)	–	(II), (III)	34.0	71.6	452 (1)
(L5)	*A′*	(II)	45	70.9	401 (1)
(L6)	*A*	(I), (II)	15.8	73.3	428 (1)
(L7)	*B*	(II), (III)	29.7	72.8	514 (1)
(L8)	–	(IV), (V), (VI)	47.1/45.0	73.8	402.7 (5)
(L9)	*A′*	(I), (II), (VII)	48.3/47.5	69.5	372 (1)
(L10)	*A*, *B*	(I)	46.8/44.9/47.3/46.2	70.7	Unknown
(L11	–	–	27.4	72.7	592 (1)

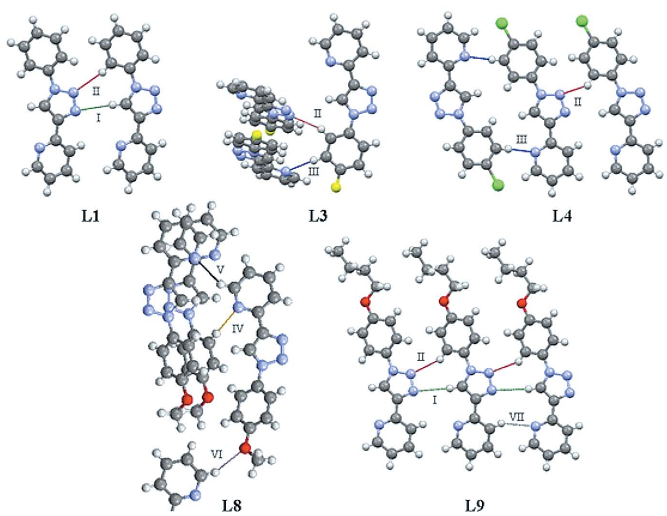

Figure 10
Examples of the seven C—H···*X* contacts identified in this work with the structures identified according to the numbering system established previously.

butoxy derivatives (L8) and (L9) crystallizing with Z' = 2 and the *N*,*N*′-dimethyl derivative (L10) containing four unique molecular geometries to give a Z' = 4 structure. *ORTEP* (Farrugia, 1997) diagrams for the novel structures characterized in this work are shown in Figs. 1–8. In all cases the pyridyl groups crystallize in the *anti*-conformation with respect to the triazole ring moiety; the molecules in (L4) and (L5) have highly dissimilar conformations in comparison with the other structures characterized in this work and this is reflected in the significant differences in intermolecular contact patterns and packing arrangements that will be discussed later.

XPac analysis using all the common non-H atoms identified two common one-dimensional arrays that are both common to three structures. The two constructs are superficially similar and correspond to a row of molecules, as shown in Fig. 9. The first, construct *A*, was identified in (L1), (L2), (L6) and (L10). Of these, (L2) and (L6) are Z' = 1 structures, (L1) is a Z' = 2 structure and (L10) is a Z' = 4 structure. In (L1) and (L10) construct *A* corresponds to the packing arrangement of only one of the molecules in the asymmetric unit. In (L1) construct *A* is formed by the molecule with an imidazole–phenyl torsion angle of 28.4 (2)° and in (L10) by the molecule with the corresponding angle of 27.2 (9)°. The second construct, *B*, was identified in (L3), (L7) and (L10). (L3) and (L7) are in fact pseudo-isostructural with a packing dissimilarity index χ = 2.7°, while in (L10) construct *B* is formed by arrays of the three molecules in the asymmetric unit other than the one that forms construct *A*. There is little obvious difference between the two supramolecular constructs in terms of the overall arrangement of the molecules and in fact when only the common non-H atoms of the pyridyl and imidazole groups were included in the analysis construct *A* in (L6) was matched to construct *B* in (L3), indicating that the two constructs are part of a continuum of packing arrangements rather than discrete entities. When the analysis was run using the common non-H atoms in the phenyl and imidazole groups this match was not made. However, a similar one-dimensional construct *A′* was identified for both of the molecules in the asymmetric units of (L1), (L9) and (L5).

Seven C—H···*X* interactions were identified by inspection of the structures using *Mercury* (Macrae *et al.*, 2008) and examples of these are shown in Fig. 10 with their geometric parameters summarized in Table 2. The most common contact is the phenyl–imidazole contact (II), which is formed in seven structures, followed by the imidazole–imidazole contact (I) in five structures and phenyl–pyridyl contact (III) in three structures. The remaining contacts (IV)–(VII) occur in individual structures and do not appear to represent robust synthons. Due to the presence of a strong carboxylic acid–pyridyl

(*a*) (*b*) (*c*)

Figure 11
Comparison of the packing arrangements of SC *A* in (*a*) (L2), (*b*) (L1) and (*c*) (L6). The structures are viewed along the axis of the $\boldsymbol{t}_1$ vector of the constructs. Constructs viewed parallel to this vector are coloured blue or black depending on their rotation about this axis and constructs viewed along the $-\boldsymbol{t}_1$ vector are shown in gold or bronze.

hydrogen bond the structure of (L11) is highly dissimilar to the others. The occurrence of the supramolecular constructs and hydrogen-bond interactions in the structures is summarized in Table 3 along with the calculated KPIs, hydrogen–hydrogen component of the Hirshfeld surfaces and experimental melting points.

Supramolecular construct *A* was identified in all three structures where (I) and (II) are the only short C—H···N contacts, indicating that this construct is a result of common directional interactions. In (L10) the construct comprises molecules linked by a longer (I) contact and (II) is absent. On visual examination the packing arrangement of the second molecule in (L1) appears to be equivalent to construct *A* with the same intermolecular contact pattern. Even with this assumed equivalence (L1) and (L2) differ markedly as shown in Fig. 11. In (L2) layers of *A* constructs along the *ac* plane lie in parallel with respect to their rotation about the $\boldsymbol{t}_1$ vector, whereas in (L1) the layers are composed of alternating pairs of *A* constructs that are rotated about the $\boldsymbol{t}_1$ axis of the vector by 180°. In (L6) the layers of *A* constructs are aligned in parallel along the crystallographic *b* and *c* axes.

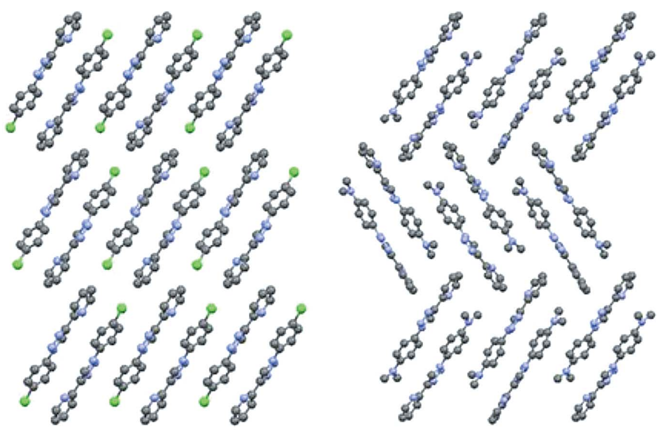

(*a*) (*b*)

Figure 12
Comparison of the packing arrangements of construct *B* in (*a*) (L3) and (*b*) (L10). The structures are viewed along the axis of the $\boldsymbol{t}_2$ translation vector and C—H···*X* contacts.

The butoxy derivative (L9) also features contacts (I) and (II) between all of the molecules to give a similar one-dimensional chain of molecules to construct (A). Similarly to (L1) this is a $Z' = 2$ structure, but in this case the structure assembles with the contacts between molecules of alternating conformations rather than separate one-dimensional chains of each conformation. This gives rise to the occurrence of contact (VII) between pairs of (9*a*) and (9*b*) molecules, resulting in the pyridyl rings lying in an alternating out-of-plane arrangement to each other. In the case of (L5) only contact (II) was identified by the search parameters in *Mercury* (Macrae *et al.*, 2008) and although the C—H···N distance for the equivalent atoms to contact (I) was of comparable length to those in (L1), (L2) and (L6), the corresponding C—H···N angle of 159° is smaller than these cases and somewhat closer to the angle observed between these atoms in (L3) and (L7). This indicates that the structure may be an intermediate form between supramolecular constructs *A* and *B* and gives further evidence for the existence of a continuum between these two groups of structures. The isostructural (L3) and (L7) both feature the phenyl–pyridyl contact (III) and phenyl–imidazole contact (IV) to two different molecules as the closest intermolecular contacts. The packing arrangements of the *B* constructs in (L3) and (L10) are compared in Fig. 12. It can be seen that in (L3) and (L7) the constructs are arranged in separated parallel layers along an axis perpendicular to the $\boldsymbol{t}_2$ translation vector, whereas in (L10) the layers stack in an antiparallel arrangement with the molecules interdigitated with the neighbouring layers. The overall structures of (L3) and (L7) are in fact highly similar to that of (L6) while (L10) mirrors the arrangement of (L1) and (L2).

Structures (L4), (L8) and (L11) all adopt unique packing arrangements with no similarity to any other structure, even when only partial fragments are used for the XPac comparisons. For (L11) this result is unsurprising, as the strong O—H···N hydrogen bond formed between the carboxylic acid and pyridyl groups is the dominant interaction, forming one-dimensional zigzag chains of molecules. The result for (L8) is perhaps unexpected given that the phenyl and imidazole groups of the butoxy analogue (8) are able to adopt a similar packing arrangement to (L1), despite the need to accommodate the larger butoxy group within the crystalline lattice. None of the previously observed C—H···N interactions can be identified in (L8) with the closest contacts being the pyridyl–

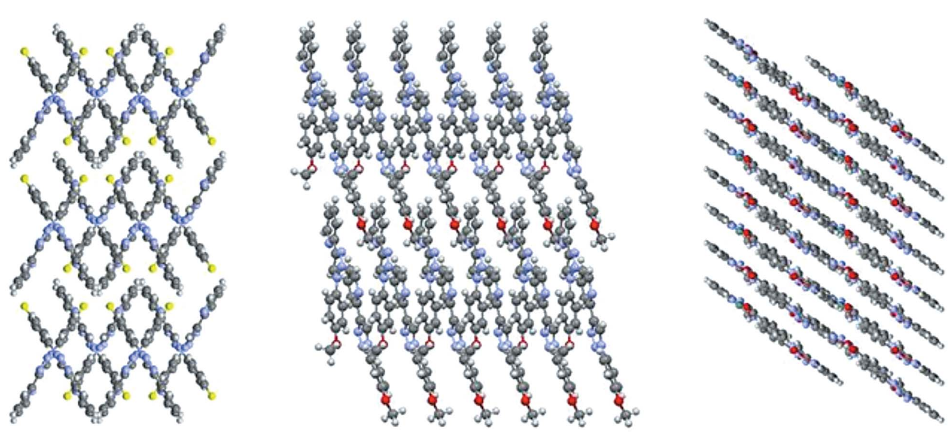

(*a*) (*b*) (*c*)

Figure 13
The unique packing arrangements adopted by (*a*) (L3), (*b*) (L8) and (*c*) (L11). (L3) and (L8) are viewed along the axis of the main hydrogen-bonding motifs shown in Fig. 1 and (L11) is viewed along the normal to the axis of the carboxylic acid–pyridyl contacts.

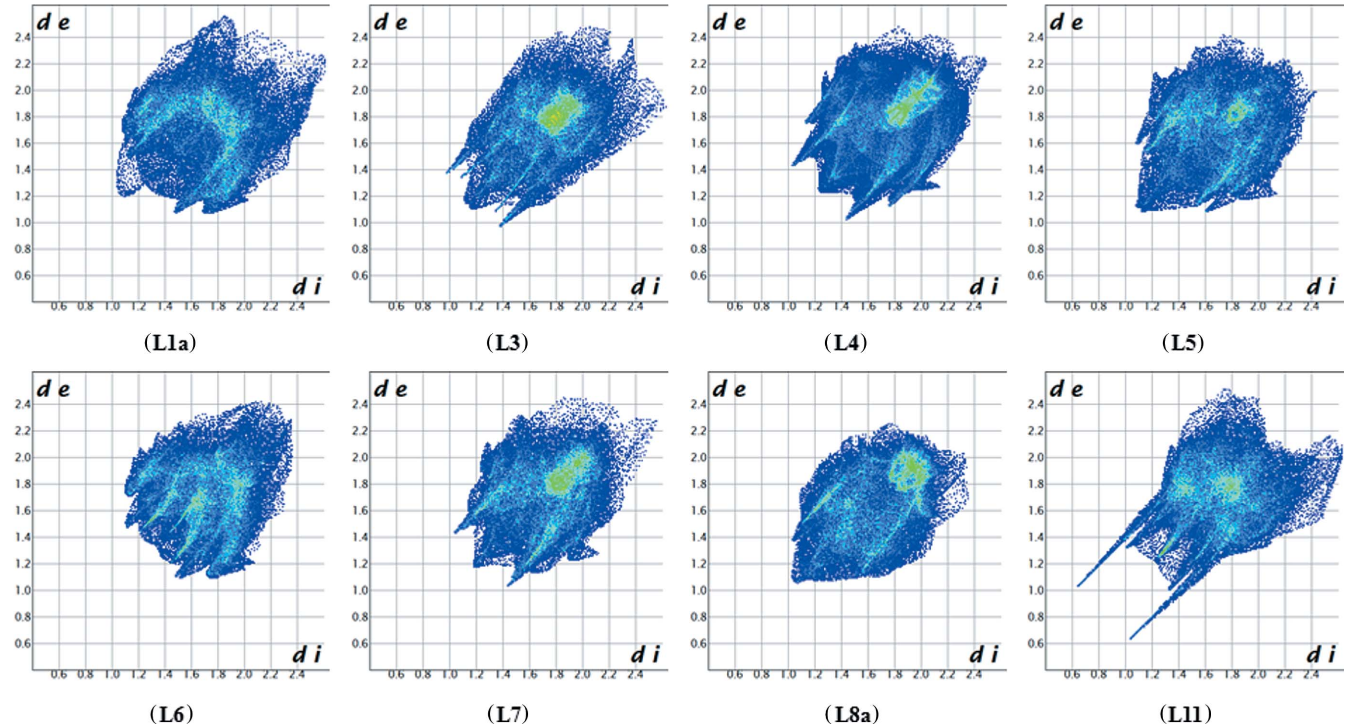

Figure 14
Examples of the two-dimensional fingerprint plots generated from the Hirshfeld surfaces calculated for the novel structures in this work. For (L1) and (L8) only one molecule from the asymmetric unit is shown.

pyridyl C—H···N contact (V) and pyridyl–methoxy C—H···O contact (VI). Not only is the fluoro derivative (L3) dissimilar to the closely related chloro derivative (L4) in terms of its intermolecular interactions and packing arrangement, but it has the most planar molecular conformation of all the molecules under examination. Each molecule donates hydrogen bonds to two molecules, forming contacts (II) and (III), respectively. In addition, C—H···F contacts align the molecules into linear chains along the axis perpendicular to the axis of these contacts. The resulting unique structural arrangements are shown in Fig. 13.

The butoxy derivative (L9) has the lowest packing efficiency with a KPI of 69.5, most probably due to the need to accommodate the butoxy group within the lattice, and it also has the highest percentage of Hirshfeld surface area accounted for by H—H contacts. This may account for the comparatively low melting point of the compound that is 30 K below that of the methoxy analogue (L8). It is unsurprising that the highest melting compound (L11) is also the only one featuring a strong intermolecular hydrogen bond as is readily apparent from a comparison of the Hirshfeld surfaces, as shown in Fig. 14. This structure also has a comparatively high KPI and low H—H contact surface area. The next three structures in order of decreasing melting point are (L7), (L3) and (L4). It is interesting to note that these structures all feature contact (III) and have the lowest percentage of Hirshfeld surface area accounted for by H—H contacts. The very low contribution of H—H contacts to the surface of (L6) is due to the significant area accounted for by H—F contacts to the trifluoromethyl groups. It can otherwise be seen in general terms that the H—H contributions to the surfaces of the remaining molecules are higher and the corresponding melting points are markedly lower.

4. Conclusions

The series of structures reported in this work illustrate the inherent unpredictability in the crystallization products of even closely related molecules and the need to bring several complementary structure analysis methods to bear on the problem. Although some relatively robust hydrogen-bond synthons could be identified, these were highly variable and significant differences were observed between the packing arrangements adopted in the crystalline state by molecules that had apparently trivial differences in molecular structure, for example in the case of the fluoro derivative (L3) and chloro derivative (L4). *XPac* analysis demonstrated that in the main the similarities in packing arrangement in the structures can be attributed to the formation of common intermolecular interactions. The physical properties of the crystals do not correlate with any single parameter, but a general trend could be identified based on the percentage of the electrostatic surface area between the molecules accounted for by H—H contacts with the melting points decreasing as the H—H area increases. The KPI values did identify cases where the accommodation of a bulky functional group compromised the packing efficiency of the molecules in the crystal structure and accounted for a significant decrease in the melting point of this system that was not accounted for by any of the other parameters under investigation.

The authors would like to thank the Iraqi Ministry for Higher Education for the providing of the funding for Mr Kinaan Tawfiq's PhD.

References

Aakeroy, C. B., Bahra, G. S., Hitchcock, P. B., Patell, Y. & Seddon, K. R. (1993). *J. Chem. Soc. Chem. Commun.* pp. 152–157.

Almarsson, O. & Zaworotko, M. J. (2004). *Chem. Commun.* pp. 1889–1896.

Alonso, F., Moglie, Y., Radivoy, G. & Yus, M. (2011). *Org. Biomol. Chem.* **9**, 6385.

Arlin, J.-B., Johnston, A., Miller, G. J., Kennedy, A. R., Price, S. L. & Florence, A. J. (2010). *CrystEngComm*, **12**, 64–66.

Bratsos, I., Urankar, D., Zangrando, E., Genova-Kalou, P., Košmrlj, J., Alessio, E. & Turel, I. (2011). *Dalton Trans.* **40**, 5188–5199.

Bruker AXS Inc. (2007), *SADABS*. Bruker AXS Inc., Madison, Wisconsin, USA.

Crowley, J. D., Bandeen, P. H. & Hanton, L. R. (2010). *Polyhedron*, **29**, 70–83.

Crowley, J. D., Kilpin, K. J., Gavey, E. L., McAdam, C. J., Anderson, C. B., Lind, S. J., Keep, C. C., Gordon, K. C. & Gordon, K. C. (2011). *Inorg. Chem.* **50**, 6334–6346.

Datta, S. & Grant, D. J. (2004). *Nat. Rev. Drug Discov.* **3**, 42–57.

Desiraju, G. R. (1997). *Chem. Commun.* pp. 1475–1482.

Dolomanov, O. V., Bourhis, L. J., Gildea, R. J., Howard, J. A. K. & Puschmann, H. (2009). *J. Appl. Cryst.* **42**, 339–341.

Farrugia, L. J. (1997). *J. Appl. Cryst.* **30**, 565.

Gelbrich, T., Hughes, D. S., Hursthouse, M. B. & Threlfall, T. L. (2008). *CrystEngComm*, **10**, 1328–1334.

Gelbrich, T. & Hursthouse, M. B. (2005). *CrystEngComm*, **7**, 324–336.

Hursthouse, M. B., Montis, R. & Tizzard, G. J. (2010). *CrystEngComm*, **12**, 953–959.

Hursthouse, M. B., Montis, R. & Tizzard, G. J. (2011). *CrystEngComm*, **13**, 3390–3401.

Kamalraj, V. K., Senthil, S. & Kannan, P. (2008). *J. Mol. Struct.* **892**, 210.

Kumar, D. & Reddy, V. B. (2010). *Synthesis*, **10**, 1687–1691.

Macrae, C. F., Bruno, I. J., Chisholm, J. A., Edgington, P. R., McCabe, P., Pidcock, E., Rodriguez-Monge, L., Taylor, R., van de Streek, J. & Wood, P. A. (2008). *J. Appl. Cryst.* **41**, 466–470.

McKinnon, J. J., Jayatilaka, D. & Spackman, M. A. (2007). *Chem. Commun.* pp. 3814–3816.

Nicolaides, A., Enyo, T., Miura, D. & Tomioka, H. (2001). *J. Am. Chem. Soc.* **123**, 2628.

Nonius (1998). *COLLECT*. Nonius BV, Delft, The Netherlands.

Odlo, K., Hentzen, J., Chabert, F. J. D., Ducki, S., Gani Osman, A. B. S. M., Sylte, I., Skrede, M., Florenes, V. A. & Hansen, T. V. (2008). *Bioorg. Med. Chem.* **16**, 4829.

Otwinowski, Z. & Minor, W. (1997). *Methods in Enzymology*, Vol. 276, *Macromolecular Crystallography*, Part A, edited by C. W. Carter Jr & R. M. Sweet, pp. 307–326. New York: Academic Press.

Palatinus, L. & Chapuis, G. (2007). *J. Appl. Cryst.* **40**, 786–790.

Park, I. S., Kwon, M. S., Kim, Y., Lee, J. S. & Park, J. (2008). *Org. Lett.* **10**, 497–500.

Park, J. W. & Park, I. S. (2011). US Patent 14.Jul:1.

Rigaku (2011). *CrystalClear-SM Expert* 2.0 r13. Rigaku Corporation, Tokyo, Japan.

Saha, B. K., Nangia, A. & Jaskolski, M. (2005). *CrystEngComm*, **7**, 355–358.

Schweinfurth, D., Hardcastle, K. I. & Bunz, U. H. F. (2008). *Chem. Commun.* pp. 2203–2205.

Schweinfurth, D., Pattacini, R., Strobel, S. & Sarkar, B. (2009). *Dalton Trans.* pp. 9291–9297.

Schweinfurth, D., Strobel, S. & Sarkar, B. (2011). *Inorg. Chim. Acta*, **374**, 253–260.

Sheldrick, G. M. (2008). *Acta Cryst.* A**64**, 112–122.

Spek, A. L. (2003). *J. Appl. Cryst.* **36**, 7–13.

Wolff, M., Munoz, L., François, A., Carrayon, Ch., Seridi, A., Saffron, N., Picard, C., Machura, B. & Benoist, E. (2013). *Dalton Trans.* **42**, 7019.

Wong, M. S., Bosshard, C. & Gunter, P. (1997). *Adv. Mater.* **9**, 554–557.